Tobacco rattle virus 16K silencing suppressor binds AGO4 and inhibits formation of RNA silencing complexes

Lourdes Fernández-Calvino[1], Llúcia Martínez-Priego[1], Edit Z. Szabo[2], Irene Guzmán-Benito[1], Inmaculada González[1], Tomás Canto[1], Lóránt Lakatos[2, 3], and César Llave[1]

[1]Department of Environmental Biology, Centro de Investigaciones Biológicas, Consejo Superior de Investigaciones Científicas, Ramiro de Maeztu 9, 28040 Madrid, Spain
[2]Department of Dermatology and Allergology, University of Szeged, H-6720 Szeged, Koranyi str. 6, Hungary
[3]MTA-SZTE Dermatological Research Group, Hungary

Running title: RNA silencing suppression by TRV 16K

Corresponding author:
César Llave; Telephone: +34-918373112; Email: cesarllave@cib.csic.es

Word count of both the summary and the main text (including the figure and table legends, in-text citations and any appendices, but not including the title page, acknowledgements, table bodies and footnotes, or reference list): 5,498
Number of figures: 5

SUMMARY

The cysteine-rich 16K protein of *Tobacco rattle virus* (TRV), the type member of the genus *Tobravirus,* is known to suppress RNA silencing. However, the mechanism of action of the 16K suppressor is not well understood. In this study, we used a GFP-based sensor strategy and the Agrobacterium-mediated transient assay in *Nicotiana benthamiana* to show that 16K was unable to inhibit the activity of existing siRNA and miRNA-programmed RISC complexes. In contrast, 16K efficiently interfered with *de novo* formation of miRNA- and siRNA-guided RISC complexes, thus preventing cleavage of target RNA. Interestingly, we found that transiently-expressed endogenous miR399 and miR172 directed sequence-specific silencing of complementary sequences of viral origin. 16K failed to bind sRNAs, albeit it interacted with AGO4 as revealed by bimolecular fluorescence complementation and immunoprecipitation assays. Site-directed mutagenesis demonstrated that highly conserved cysteine residues within the N-terminal and central regions of the 16K protein were required for protein stability and/or RNA silencing suppression.

INTRODUCTION

Tobacco rattle virus (TRV) is a bipartite single-stranded (ss), positive sense RNA plant virus and the type member of the genus *Tobravirus* (family *Virgaviridae*) (Macfarlane, 2010). TRV is an important pathogen of cultivated potato, although it infects a wide range of plant species, including the model plants *Nicotiana benthamiana* and *Arabidopsis thaliana* (Fernandez-Calvino *et al.*, 2014).

TRV infection is tightly controlled by RNA silencing as deduced by elevated TRV levels in plants in which RNA silencing components are genetically inactivated (Donaire *et al.*, 2008). ARGONAUTE (AGO) proteins are core components of RNA-induced silencing effector complexes (RISC) that use small RNA (sRNA) to silence complementary RNA through translational repression and/or RNA slicing (Brodersen & Voinnet, 2006; Vaucheret, 2008). A programmable small interfering RNA (siRNA)-containing antiviral AGO complex is triggered upon TRV infection to selectively cleave viral RNA (Ciomperlik *et al.*, 2011). Several studies identified the TRV-encoded 16K protein as the main suppressor of RNA silencing (Ghazala *et al.*, 2008; Martin-Hernandez & Baulcombe, 2008; Martinez-Priego *et al.*, 2008), although the 29K movement protein also contributes to suppression of RNA silencing in the context of viral replication (Deng *et al.*, 2013). 16K is primarily cytoplasmic although it can be found to a lower extent in the nucleus, coinciding with the existence of two functional bipartite nuclear localization signals in the protein (Ghazala *et al.*, 2008; Liu *et al.*, 1991). In plants, 16K suppresses RNA silencing induced by ssRNA as well as low concentration of double-stranded (ds) RNA, and reduces the accumulation of siRNAs in both transient and stable expression assays (Ghazala *et al.*, 2008; Martin-Hernandez & Baulcombe, 2008; Martinez-Priego *et al.*, 2008). Interestingly, TRV accumulates and propagates systemically without 16K in wild-type plants (Deng *et al.*, 2013; Martin-Hernandez & Baulcombe, 2008). Yet, TRV mutants carrying a dysfunctional 16K gene exhibit appreciable

differences in their accumulation dynamics with respect to the wild-type virus (Deng *et al.*, 2013), cause necrotic symptoms in inoculated and systemically infected leaves (Deng *et al.*, 2013; Martin-Hernandez & Baulcombe, 2008), and are unable to invade meristems (Martin-Hernandez & Baulcombe, 2008). Besides, 16K supports synergistic effects on virus-double infections (Andika *et al.*, 2012) and contributes to stabilize the genomic RNA2 of TRV (Deng *et al.*, 2013). In this paper, we want to gain insights into the mechanism of suppression of 16K using the agrobacterium-mediated transient assay in *N. benthamiana*.

RESULTS

16K does not inhibit activity of miRNA and viral siRNA-programmed RISC complexes

To investigate whether 16K inhibits active (assembled) miRNA-loaded RISC complexes, we used the agrobacterium-mediated transient assay in *N. benthamiana* to express a GFP-based sensor construct, driven by the 35S *Cauliflower mosaic virus* (CaMV) promoter, with or without viral suppressor. The GFP-171.1 sensor contained a full complementary miR171-binding site immediately downstream of the stop codon of GFP allowing miR171-mediated silencing of the GFP-171.1 mRNA (Parizotto *et al.*, 2004). GFP expression in the infiltrated zone was compared to that of leaves in which GFP-171.1 was coinfiltrated with *Tobacco etch potyvirus* (TEV) HC-Pro or *Sweet potato mild mottle ipomovirus* (SPMMV) P1 silencing suppressor that was used as control. The HC-Pro has no effect on miRNA- and siRNA-loaded RISCs, whereas P1 inhibits miRNA-programmed RISC activity (Giner *et al.*, 2010; Lakatos *et al.*, 2006). In our assays, GFP fluorescence was detected under UV light at comparable low levels in leaves infiltrated with 16K, HC-Pro or empty vector at 2 days post-infiltration (dpi) (Fig 1a). In contrast, leaves agroinjected with P1 showed a marked increase in green fluorescence as a result of P1-mediated interference on miR171-guided cleavage of the GFP-171.1 mRNA (Fig 1a). GP171.1 mRNA and protein accumulated to the same levels in

89 samples injected with 16K, HC-Pro or empty vector, whereas they accumulated to higher
90 levels when P1 was co-delivered in the patch (Fig 1b). Therefore, 16K, like HC-Pro, failed to
91 inhibit the activity of miR171-loaded active RISC complexes.
92 Next, we wondered if 16K may inhibit viral siRNA-loaded active silencing complexes. To
93 test this possibility we used plants infected systemically with a *Cymbidium ringspot*
94 *tombusvirus* (CymRSV) 19 Stop mutant (Cym19S), which does not express the P19 silencing
95 suppressor (Szittya *et al.*, 2002). These plants display a phenotype of recovery due to the
96 activation of a strong RNA silencing response that implicates the processing activity of viral
97 siRNA-loaded AGO complexes against the virus (Silhavy *et al.*, 2002; Szittya *et al.*, 2002).
98 The sensor construct GFP-Cym, which contains a ~200 bp portion of the CymRSV RNA
99 fused after the GFP stop codon, is susceptible of cleavage by RISC complexes containing
100 viral siRNAs (Giner *et al.*, 2010; Lakatos *et al.*, 2006). The GFP-PoLV, in which GFP is
101 fused with a ~200 bp portion of *Pothos latent aureusvirus* (PoLV), was used as a negative
102 control (Pantaleo *et al.*, 2007). Recovering leaves of Cym19S-infected plants were then
103 infiltrated with GFP-Cym or GFP-PoLV alone or with the indicated silencing suppressors.
104 Visual inspection of GFP fluorescence showed that GFP-Cym, but not the non-target GFP-
105 PoLV sensor, was down-regulated by RNA silencing against Cym19S (Fig 1c). Moreover
106 neither HC-Pro nor 16K were able to elevate the accumulation of the cognate sensor (GFP-
107 Cym), while patches infiltrated with the non-cognate sensor showed much brighter
108 fluorescence. In contrast, GFP fluorescence was strong in patches infiltrated with GFP-Cym
109 or GFP-PoLV together with P1 indicating suppression of RNA silencing (Fig 1c).
110 Co-expression of the GFP-Cym construct with 16K or HC-Pro in infected leaves resulted in
111 the accumulation of full-length mRNA along with a shorter 3' RNA cleavage product that
112 originated from viral siRNA-directed processing of the complementary region in the GFP-
113 Cym mRNA (Fig 1d). In contrast, a unique hybridization band corresponding to the intact

full-length mRNA was detected in tissues injected with the non-homologous GFP-PoLV (Fig 1d). Accordingly, GFP-PoLV protein levels were higher than the GFP-Cym levels (Fig 1d). Therefore, 16K was not competent to interfere with viral siRNA-programmed active RISC complexes and to prevent cleavage of the GFP-Cym sensor RNA. GFP mRNA and protein levels were similar in samples injected with GFP-Cym or GFP-PoLV in the presence of P1, which is known to inhibit slicing activity of viral siRNA-containing AGO complexes (Fig 1d). Furthermore, no cleavage products of GFP were found in samples co-infiltrated with the GFP-Cym and P1 constructs.

16K interferes with *de novo* formation of RISC and target cleavage

We investigated if 16K interferes with RISC assembly to prevent subsequent target cleavage using two possible targeting scenarios: host sequences and viral sequences (Kasschau *et al.*, 2003). We used a GFP-based sensor strategy to test functional miRNA-target interactions. Given that miR171-containing AGO complexes exist in the *N. benthamiana* leaves prior to agroinfiltration, we generated a novel reporter to test this hypothesis. The validated binding site of miR172 as found in *Apetala 2* (*AP2*) (Chen, 2004) was placed immediately after the GFP ORF stop codon (Fig 2a). The resultant GFP-AP2 construct was agro-injected either alone, with an empty vector or with a MIR gene. The observation of bright fluorescence in patches containing GFP-AP2 and empty vector validated our sensor assay and ruled out a potential regulatory effect driven by preassembled endogenous miR172 (Fig 2b). When GFP-AP2 was delivered in the presence of empty vector or heterologous miRNAs (miR399, miR158 or miR171), GFP fluorescence and GFP-AP2 transcript levels in the infiltrated zone were comparable to those of a native GFP construct (Fig 2b, c). In contrast, fluorescence virtually disappeared and GFP-AP2 mRNA remained below detection limits when the GFP-AP2 sensor was co-injected with the cognate miR172-expressing construct, presumably due

139 to miR172-mediated cleavage of the GFP-AP2 mRNA (Fig 2b, c). Interestingly, restoration of
140 green fluorescence and GFP-AP2 mRNA levels in the presence of 16K or HC-Pro indicated
141 that miR172-guided silencing was partially abolished (Fig 2b, c). These results suggested that
142 16K interferes with the proper formation and subsequent function of AGO-containing effector
143 complexes.
144 Next we tested the ability of 16K to perturb host miRNA programming and targeting against
145 viral sequences. To test the idea, we first investigated if host miRNAs promote
146 endonucleolytic cleavage of complementary viral sequences. We took advantages of our
147 validated miR172-targeting system, and hence the mature miR172 sequence was used as a
148 query to search for potential targets in a collection of viral genomes using the Small RNA
149 Target Prediction program (Jones-Rhoades & Bartel, 2004). This analysis identified the
150 genome of *Maize chlorotic dwarf virus* (MCDV) as comprising potential miR172-binding
151 sites (Fig 3a). We also searched for host miRNAs that base-pair with the TRV genome and
152 identified miR399 as a candidate interactor (Fig 3a).
153 A stretch of 30 nts harboring each of the target viral sequences was fused to the GFP ORF
154 immediately after the stop codon. The resulting GFP-MCDV and GFP-TRV constructs were
155 expressed either alone or in combination with miRNA-containing constructs as shown above.
156 Green fluorescence was detected in patches infiltrated with GFP-MCDV plus empty vector or
157 heterologous miRNAs (miR399, miR158 and miR171) to levels similar to those observed in
158 tissue expressing the wild-type GFP alone (Fig 3b). This finding excluded a potential effect of
159 pre-assembled miR172-guided complexes against GFP-MCDV transcripts. In contrast, GFP
160 expression was turned off when GFP-MCDV was co-delivered with a miR172-containing
161 construct (Fig 3b). GFP-MCDV mRNA was drastically diminished in the presence of miR172
162 owing to miR172-triggered post-transcriptional silencing (Fig 3b). Green fluorescence was
163 observed in patches holding GFP-TRV and empty vector or heterologous miRNAs (miR158

and miR171), but was notably reduced when GFP-TRV was co-delivered with miR399 (Fig 3c). Accordingly, GFP-TRV mRNA accumulated to lower level if miR399 was co-expressed in the agro-infiltrated leaves (Fig 3c). As it would be anticipated, both 16K and HC-Pro interfere with *de novo* formation of miRNA complexes and suppress miRNA-mediated silencing, irrespective of the origin of the target sequences, restoring green fluorescence derived from GFP-MCDV to nearly wild-type levels (Fig 3b).

Selective binding to sRNAs represents the basis for inhibition of RISC assembly and target cleavage by multiple viral proteins (Lakatos *et al.*, 2006). We examined *in vitro* if 16K was capable of binding ds-sRNAs. Crude extracts of *N. benthamiana* leaves expressing a silencing suppressor-competent 16K were incubated with ^{32}P-labeled synthetic 21-nt ds siRNAs, and the complexes were resolved on a native electrophoresis gel. P19 from *Tomato bushy stunt virus* (TBSV) was used as a binding control. As expected, the P19 control bound dsRNA as evidenced by a shift in siRNA mobility due to the formation of P19-siRNA complexes (Fig 2d). No siRNA binding could be inferred from leaves expressing either empty vector or 16K (Fig 2d).

16K physically interacts with AGO4

To test if the 16K silencing suppressor interacts physically with AGO proteins, we used bimolecular fluorescence complementation (BiFC) to monitor *in vivo* protein-protein interactions. When sYFPN-tagged proteins were coinfiltrated with an empty sYFPC construct or when the sYFPC-tagged proteins were coexpressed with a construct expressing a sYFPN alone, no fluorescence could be detected (data not shown). At 3 dpi, we found that the 16K protein interacted strongly with itself in *N. benthamiana* epidermal cells. The fluorescence derived from the reconstitution of the YFP fluorophore was predominately cytoplasmic although nucleolus-associated fluorescence was detected within the nucleus (Fig 4a). Our

BiFC assay revealed reconstitution of YFP fluorophore, mostly localized in the cytoplasm, in samples co-agroinjected with sYFPN-16K and sYFPC-AGO1, suggesting a 16K-AGO1 association (Fig 4b). However, AGO1 binding could not be validated by immunoprecipitation (IP) assays using different tagged-protein combinations (data not shown). Interestingly, BiFC suggested a cytoplasmic association of 16K with AGO4 that was further validated by IP using a HA-tagged version of 16K and a sYFPN-AGO4 construct (Fig 4b). At 3 dpi, extracts were prepared from infiltrated leaves and HA-tagged 16K was immunoprecipiated with an anti-HA antibody. The 16K protein was detected by Western blot using an anti-HA antibody in all samples tested indicating that HA-16K could be immunoprecipitated from extracts (Fig 4b). Using an anti-GFP antibody, we found that sYFPN-AGO4 coimmunoprecipitated with HA-16K, confirming that the interaction was specific (Fig 4b).

To test if sYFP tagging of 16K affects its ability to suppress local silencing, we interrogated the sYFPN-16K or sYFPC-16K constructs used in BiFC in the transient GFP-based silencing assay. Patches infiltrated with GFP and sYFPN-16K or sYFPC-16K showed a marked increase in green fluorescence that was comparable to that observed in the presence of the native 16K protein (Fig 4c). Furthermore, suppression of GFP silencing was also evident upon transient co-expression of GFP with an inverted-repeat dsGFP construct, demonstrating that sYFP tagging of 16K did not compromise its silencing suppression properties (Fig 4c).

Mutations on conserved cysteines of 16K affect protein accumulation and silencing suppressor activities

The 16K gene of tobraviruses encodes a protein with N-terminal and central Cys-rich motifs reminiscent of zinc-finger domains present in some regulatory proteins (Fig 5a) (Liu *et al.*, 2002). Comparison of 16K with other Cys-rich proteins from furoviruses, hordeiviruses and pecluviruses identified a central highly conserved Cys-Cys-Gly-X-X-His pattern (Fig 5a)

214 (Diao *et al.*, 1999). We wanted to investigate the significance of the Cys residues within the
215 conserved N-terminal and central motifs of 16K on protein stability, silencing suppression
216 and AGO4 binding. We used site-directed mutagenesis to generate: i) a 16K deletion mutant
217 that lacked the Cys-containing first N-terminal 17 amino acids, and ii) a double 16K mutant
218 in which Cys at amino acid positions 65 and 66 were replaced with phenylalanine (Fig 5a).
219 The resulting 16KΔ17 and 16KC65-66/P mutants were fused to the sYFPN half to create
220 sYFPN-16KΔ17 and sYFPN-16KC65-66/P recombinant proteins, respectively.
221 We first investigated if the sYFPN-16K mutant proteins retained the ability to block intrinsic
222 silencing triggered by T-DNA expression. Silencing suppressor activity of the sYFPN-tagged
223 16K mutants was compared to sYFPN-16K using the agroinfiltrated patch silencing
224 suppression assay in *N. benthamiana* at 5 dpi. Northern bot revealed a subtle increased in
225 GFP transcripts in patches co-infiltrated with GFP and sYFPN-16KΔ17 and sYFPN-16KC65-
226 66/P compared to control plants injected with empty vector, suggesting a partial inhibition of
227 GFP silencing (Fig 5b). However, the extent to which GFP silencing was suppressed by both
228 mutants was far less than that observed in plants infiltrated with the native sYFPN-16K (Fig
229 5b). Visual inspection under UV light at 5 dpi revealed decreased green fluorescence in
230 patches co-infiltrated with GFP and sYFPN-16KΔ17, sYFPN-16KC65-66/P or empty vector
231 relative to sYFPN-16K (Fig 5c).
232 To test if the above mutations affected protein stability, we compared accumulation of 16K
233 mutant proteins relative to wild-type 16K. The sYFPN-tagged 16K-derived constructs were
234 agroinfiltrated at OD_{600} of 0.1 or 0.3 and proteins were extracted at 3 dpi and analyzed by
235 Western blot using the N-terminal half GFP antibody. Densitometric analysis of several
236 independent replicates revealed that sYFPN-16KC65-66/P accumulated between 40 to 70%
237 less than the sYFPN-16K control (a representative blot is shown in Fig. 5d). In most cases,
238 the accumulation of sYFPN-16KΔ17 in the transient assay was reduced by nearly 40%

compared to sYFPN-16K, although we occasionally detected similar protein accumulation in leaves infiltrated with sYFPN-16K or sYFPN-16KΔ17 (Fig 5e). Low protein levels in our assay could be interpreted as protein instability caused by the 16KΔ17 and C65-66/P mutations. Alternatively, it can be a consequence of the mutants' inability to suppress local silencing triggered by T-DNA expression. We found that sYFPN-16KΔ17 protein levels were significantly elevated when a functional P19 suppressor was transiently co-delivered, indicating that the suppressor-deficient sYFPN-16KΔ17 protein was stable provided that silencing was counteracted by P19 (Fig 5e). This finding suggests that the failure of sYFPN-16KΔ17 to suppress local transgene silencing causes a negative feedback inhibition on its own production, which in turn, leads to reduced GFP expression. In contrast, sYFPN-16KC65-66/P proteins remained to low levels irrespective of P19, pointing to a dramatic impact of this mutation on protein accumulation that indirectly results in a dysfunctional suppressor of silencing (Fig 5e).

We failed to detect YFP fluorescence derived from the BiFC of transiently expressed sYFPN-16K mutants and sYFPC-AGO4 (Fig 5f). Likewise, we could not appreciate self-association of sYFPN- and sYFPC-tagged 16K mutant constructs (data not shown). Given that both C65-66/P and 16KΔ17 mutations affected protein accumulation, we cannot unambiguously discriminate whether the lack of BiFC-derived YFP fluorescence was due to poor protein levels in the injected tissue or inability of mutated proteins to interact.

The 16K suppressor of TRV possesses a single glycine/tryptophane (GW) motif at position 48 within the N-terminal half. GW/WG repeats have been identified in viral suppressors of silencing, and they can act as AGO hooks essential for AGO binding (Azevedo *et al.*, 2010; Giner *et al.*, 2010; Karlowski *et al.*, 2010). Using a 16K construct carrying a GW→GA point mutation, we found however that this predicted GW motif was irrelevant for silencing suppressor in the transient assay (Fig 5b, c).

DISCUSSION

In this study we aimed to better understand the molecular basis of the 16K-mediated inhibition of RNA silencing. Our results indicated that, in the transient assay, 16K was unable to block cleavage of a GFP sensor mRNA by a pre-existing miRNA/siRNA-programmed RISC. However, 16K successfully prevented miRNA-guided cleavage of target RNAs when both the miRNA and the sensor constructs were simultaneously co-delivered into the plant tissue. This suggested that 16K presumably acted by impeding initial RISC assembly. The P19, p21 and HC-Pro viral suppressors, which primarily block RISC programming, use sRNA sequestration as a means to prevent sRNA incorporation into AGO (Burgyan & Havelda, 2011; Garcia-Ruiz *et al.*, 2015; Lakatos *et al.*, 2006; Schott *et al.*, 2012). As opposed to these suppressors, the basis for the inhibition of RISC formation by 16K was not related to sRNA sequestration as 16K failed to bind siRNAs. However, it is conceivable that 16K could affect RISC assembly by compromising sRNA availability as 16K causes reduced accumulation of silencing-associated siRNAs (Ghazala *et al.*, 2008; Martinez-Priego *et al.*, 2008). Alternatively, 16K could perturb RISC assembly by interfering with AGO proteins. Our BiFC assay suggested a potential interaction between 16K and AGO1 that could not be however validated by IP. In contrast, we found compelling evidence that 16K associates with AGO4. miR172 harbors a 5'-terminal adenosine and binds AGO4 to direct effective cleavage of *AP2* mRNA targets *in vitro* (Qi *et al.*, 2006). These findings suggest a productive role for AGO4 in our transient silencing assay. However, whether 16K interferes with *de novo* formation of RISC via AGO4 binding remains to be tested.

Here, we found roles for AGO2 and AGO4 in susceptibility to TRV, whereas AGO1 targeting of TRV is unclear as suggested by the erratic accumulation of TRV in *ago1-27* mutants observed using qRT-PCR and Western blot (Fig 4d). These observations have been recently

289 corroborated by others (Carbonell & Carrington, 2015; Ma *et al.*, 2015) and suggest that
290 AGO2 and AGO4 are the two major antiviral AGOs against TRV. The raising question is
291 whether 16K association with AGO4 alleviates antiviral effects during TRV infection.
292 Despite AGO4 normally functions in transcriptional gene silencing by guiding
293 hypermethylation of target DNA, it plays an antiviral role against several RNA viruses that is
294 likely related to RNA slicing (Carbonell & Carrington, 2015). Direct physical interaction of
295 viral silencing suppressors with AGO4 has been reported in consistency with their ability to
296 block the *in vitro* slicer activity of AGO4 (Hamera *et al.*, 2012; Perez-Canamas & Hernandez,
297 2015). Furthermore, AGO4-mediated cleavage-independent control of viral translation has
298 been shown to modulate virus resistance induced by NB-LRR protein in *N. benthamiana* s
299 (Bhattacharjee *et al.*, 2009).
300 The 16K protein is a small Cys-rich protein that shares sequence homology with Cys-rich
301 proteins of *Furovirus*, *Hordeivirus*, *Pecluvirus*, *Benyvirus* and *Carlavirus*. In
302 complementation studies, the *Soilborne wheat mosaic furovirus* (SBWMV) 19K or the *Barley*
303 *stripe mosaic hordeivirus* (BSMV) γb protein functionally replaced the 16K of TRV,
304 indicating that Cys-rich proteins likely share common functions (Liu *et al.*, 2002). In fact,
305 BSMV γb, the SBWMV 19K, and *Peanut clump pecluvirus* (PCV) 15K proteins are known to
306 suppress RNA silencing and modulate symptom severity and systemic virus accumulation
307 (Donald & Jackson, 1994; Dunoyer *et al.*, 2002; Te *et al.*, 2005; Yelina *et al.*, 2002). We
308 found that the highly conserved Cys residues at the N-terminal segment of 16K were critical
309 for protein stability and function. Whereas the lack of suppression by sYFPN-16KC65-66/P
310 was likely due to protein instability incurred by the double C65-66/P mutation, the 16KΔ17
311 deletion rendered a suppression-deficient protein that was unable to repress local silencing
312 triggered by T-DNA expression. It would be interesting to test if mutations on these
313 conserved Cys residues disrupted the formation of the zinc finger structure leading to

314 improper protein folding. Also, future research should be conducted to determine the effects
315 of Cys mutations in the context of TRV infection.
316 Our results depicts a scenario whereby host sRNAs hold the potential to down-regulate viral
317 genomes (Lin *et al.*, 2009; Llave, 2004; Niu *et al.*, 2006; Simon-Mateo & Garcia, 2006). We
318 proved that miR172 and miR399 dampen expression of GFP sensors carrying complementary
319 sequences from MCDV and TRV genomes, respectively. It is worth noting that the selected
320 miR172:GFP-MCDV RNA duplex has only moderate complementarity with two central
321 mismatches. This indicates that perfect central complementarity is not compulsory for target
322 recognition and mRNA clearing, and that factors others than sequence complementarity at the
323 binding site could influence the outcome of silencing. This agrees with a recent paper by (Li
324 *et al.*, 2014) in which they demonstrated that perfect central complementarity is not required
325 for strong silencing. Furthermore, they appraised of differences in the miRNA:target mRNA
326 stoichiometry and the context in which the miRNA binding site resides as key determinants in
327 controlling the degree of silencing (Li *et al.*, 2014; Todesco *et al.*, 2010). The putative
328 miR399 binding site within TRV RNA1 includes one mismatch at the 5' seed region and one
329 mismatch and three non-canonical G:U pairs at the 3' end. Although the miR399-TRV
330 pairing apparently satisfies the canonical parameters for miRNA target recognition
331 (Brodersen & Voinnet, 2009; Palatnik *et al.*, 2003; Schwab *et al.*, 2005), the complementarity
332 is only partial. It is important to bear in mind that in our experimental conditions elevated
333 miR172 and miR399 levels in the infiltrated area may boost targeting efficiency under
334 suboptimal miRNA-target complementarity (Li *et al.*, 2014; Todesco *et al.*, 2010).
335 The challenge ahead is to investigate if host miRNAs target genuine viral sequences in the
336 context of the infection. Two lines of evidence are in support of this idea. First, *Arabidopsis*
337 miRNAs negatively regulate plant virus chimeras bearing miRNA target sequences (Simon-
338 Mateo & Garcia, 2006). Second, *Arabidopsis* plants transformed with recombinant miRNA

precursors engineered to contain complementary viral sequences become specifically immune to infection with these viruses (Lin *et al.*, 2009; Niu *et al.*, 2006). Under natural conditions, however, it is still unclear whether interactions involving naturally-occurring miRNAs and viral genomes have petty effects on the infection or, in contrast, they have a dynamic role in avoiding excessive virus proliferation during infection. (Qu *et al.*, 2008). We cannot rule out that fortuitous interactions between functional miRNAs and viral sequences encoding indispensable functional domains could contribute to shape the outcome of certain plant-virus pathosystems. However, the observation that viruses rapidly evolve their genomes in order to avoid miRNA recognition argues against the efficacy of miRNAs as antiviral regulators in plants (Lin *et al.*, 2009; Simon-Mateo & Garcia, 2006).

METHODS

Plant material and transient expression assay. Transient expression was conducted in *N. benthamiana* plants grown under 16h/8h light/dark and 25ºC. Arabidopsis plants were grown under 16h/8h light/dark at 19-22ºC. The Arabidopsis homozygous *ago1-27*, *ago2-1* and *ago4-2* were donated by James C. Carrington (The Donald Danforth Plant Center, Missouri, USA). TRV inoculation of Arabidopsis was done as described (Fernandez-Calvino *et al.*, 2014). Agroinfiltration of *N. benthamiana* leaves was performed as described (Johansen & Carrington, 2001). Unless otherwise indicated, cultures containing GFP-based constructs were infiltrated at OD_{600}= 0.1 or 0.2, viral suppressors at OD_{600}= 0.3, and cultures harboring miRNA constructs at OD_{600}= 0.6. Cultures carrying sYFPN- and sYFPC-tagged proteins were coinfiltrated each at OD_{600}= 0.2. The final concentration of bacteria was normalized to OD_{600}= 0.5 or 1.0 by varying the concentration of cells containing empty vector.

RNA analysis. Total RNA was extracted with the TRIZOL reagent (Invitrogen). Denaturing

gel blot hybridization of normalized total RNA was done as described previously (Martinez-Priego *et al.*, 2008). Radiolabeled DNA probes were synthesized by random priming using [α-^{32}P] dCTP. Oligonucleotides complementary to Arabidopsis miRNAs were end-labeled with [γ-^{32}P] ATP. One-step qRT-PCR reactions using β-tubulin (At1g20010) transcripts for normalization were done using as described (Fernandez-Calvino *et al.*, 2015). A list of primers used in this study is provided as supplemental Table S1.

IP and protein analysis. IP assays were done as described (Chapman *et al.*, 2004). Protein extracts were prepared and analyzed by immunoblot assay after SDS-PAGE with a rabbit anti-GFP or anti-HA antibodies (González *et al.*, 2010; Lakatos *et al.*, 2006). Blotted proteins were detected using commercial horseradish peroxidase-conjugated secondary antibodies and a chemiluminescent substrate (LiteAblot, Italy).

Vector DNA constructs for BiFC assays. Proteins were cloned into pROK2-based vectors containing the sYFPN- and sYFPC-terminal halves as described (González *et al.*, 2010). The 16K mutants (Δ17, C65/66P, and GW/GA) were engineered by conventional PCR site-directed mutagenesis. The coding sequence of AGO1 (At1g48410) and AGO4 (At2g27040) were amplified from Arabidopsis mRNA. All constructs were authenticated by DNA sequencing.

GFP sensors and miRNA-containing DNA constructs for transient expression assays. The 35S-GFP-miR171.1, 35S-GFP-Cym, 35S-GFP-PoLV, 35S-HA-16K, 35S-P19, 35S-P1/HC-Pro, and 35S-MIR171a constructs were described (Canto *et al.*, 2006; Giner *et al.*, 2010; Llave *et al.*, 2002; Martinez-Priego *et al.*, 2008; Parizotto *et al.*, 2004). The remaining 35S-driven constructs were done using the binary vector pSLJ75I55 and then introduced into

389 *Agrobacterium tumefaciens* strain GV2260. For GFP-based constructs, the soluble modified
390 GFP cDNA was PCR-amplified using reverse tagged-primers that contained the validated
391 *AP2* (At4g36920) miRNA target sequence, or the viral complementary sequences as found in
392 the genome of the Tennessee isolate of MCDV (NC_0036626; coordinates 11628-11648) or
393 the PpK20 isolate of TRV (NC_003805; coordinates 2418-2437). The MIR158a, MIR172b
394 and MIR399b genes were PCR-amplified from Arabidopsis genomic DNA using gene
395 specific primers. All constructs generated were verified by DNA sequencing.
396
397 **Electrophoretic mobility shift assay (EMSA).** EMSA was done as described (Csorba &
398 Burgyan, 2011) using synthetic siRNAs (5'-CGUACGCGUCACGCGUACGUU-3' and 5'-
399 CGUACGCGUGACGCGUACGUU-3') (Sigma) labeled with [γ-^{32}P] ATP.
400
401 **Confocal microscopy.** Plant tissue was imaged using a Olympus SZX12 stereomicroscope
402 and a Leica TCS SP5 inverted confocal microscope with an Argon ion laser. GFP was excited
403 at 488 nm and the emitted light captured at 505 to 555 nm. YFP was excited at 514 nm, and
404 the emitted light was captured at 525–650 nm.
405
406 **ACKNOWLEDGMENTS**
407 This work was supported by grants BIO2006-13107 and BIO2009-12004 from the Spanish
408 Ministry of Science and Innovation (MICINN-FEDER funding program) (CL), grants OTKA
409 NN 107787 and NN 111024 from the Hungarian Scientific Research Fund and (LL), and
410 grant AGL2008-03482 from MICINN (TC). LFC was the recipient of a JAE-Doc Contract
411 from CSIC. IGB and IG were supported by graduate fellowships from MICINN. LL was
412 supported from TÁMOP-4.2.2.A11/1/KONV-2012-0035. We thank Livia Donaire, M. Teresa

413 Seisdedos and Mónica Fontenla for technical assistance and critical comments on this
414 manuscript.
415 All authors have no conflicting financial or commercial interests.
416

417 **REFERENCES**

418 **Andika, I. B., Kondo, H., Nishiguchi, M. & Tamada, T. (2012).** The cysteine-rich proteins
419 of Beet necrotic yellow vein virus and Tobacco rattle virus contribute to efficient
420 suppression of silencing in roots. *J Gen Virol* **93**, 1841-1850.

421 **Azevedo, J., Garcia, D., Pontier, D., Ohnesorge, S., Yu, A., Garcia, S., Braun, L.,**
422 **Bergdoll, M., Hakimi, M. A., Lagrange, T. & Voinnet, O. (2010).** Argonaute
423 quenching and global changes in Dicer homeostasis caused by a pathogen-encoded GW
424 repeat protein. *Genes Dev* **24**, 904-915.

425 **Bhattacharjee, S., Zamora, A., Azhar, M. T., Sacco, M. A., Lambert, L. H. & Moffett, P.**
426 **(2009).** Virus resistance induced by NB-LRR proteins involves Argonaute4-dependent
427 translational control. *Plant J* **58**, 940-951.

428 **Brodersen, P. & Voinnet, O. (2006).** The diversity of RNA silencing pathways in plants.
429 *Trends Genet* **22**, 268-280.

430 **Brodersen, P. & Voinnet, O. (2009).** Revisiting the principles of microRNA target
431 recognition and mode of action. *Nat Rev Mol Cell Biol* **10**, 141-148.

432 **Burgyan, J. & Havelda, Z. (2011).** Viral suppressors of RNA silencing. *Trends Plant Sci* **16**,
433 265-272.

434 **Canto, T., Uhrig, J. F., Swanson, M., Wright, K. M. & MacFarlane, S. A. (2006).**
435 Translocation of Tomato bushy stunt virus P19 protein into the nucleus by ALY proteins
436 compromises its silencing suppressor activity. *J Virol* **80**, 9064-9072.

Carbonell, A. & Carrington, J. C. (2015). Antiviral roles of plant ARGONAUTES. *Curr Opin Plant Biol* **27**, 111-117.

Chapman, E. J., Prokhnevsky, A. I., Gopinath, K., Dolja, V. V. & Carrington, J. C. (2004). Viral RNA silencing suppressors inhibit the microRNA pathway at an intermediate step. *Genes Dev* **18**, 1179-1186.

Chen, X. (2004). A microRNA as a translational repressor of APETALA2 in Arabidopsis flower development. *Science* **303**, 2022-2025.

Ciomperlik, J. J., Omarov, R. T. & Scholthof, H. B. (2011). An antiviral RISC isolated from Tobacco rattle virus-infected plants. *Virology* **412**, 117-124.

Csorba, T. & Burgyan, J. (2011). Gel mobility shift assays for RNA binding viral RNAi suppressors. *Methods Mol Biol* **721**, 245-252.

Deng, X., Kelloniemi, J., Haikonen, T., Vuorinen, A. L., Elomaa, P., Teeri, T. H. & Valkonen, J. P. (2013). Modification of Tobacco rattle virus RNA1 to serve as a VIGS vector reveals that the 29K movement protein is an RNA silencing suppressor of the virus. *Mol Plant Microbe Interact* **26**, 503-514.

Diao, A., Chen, J., Ye, R., Zheng, T., Yu, S., Antoniw, J. F. & Adams, M. J. (1999). Complete sequence and genome properties of Chinese wheat mosaic virus, a new furovirus from China. *J Gen Virol* **80 (Pt 5)**, 1141-1145.

Donaire, L., Barajas, D., Martinez-Garcia, B., Martinez-Priego, L., Pagan, I. & Llave, C. (2008). Structural and genetic requirements for the biogenesis of tobacco rattle virus-derived small interfering RNAs. *J Virol* **82**, 5167-5177.

Donald, R. G. & Jackson, A. O. (1994). The barley stripe mosaic virus gamma b gene encodes a multifunctional cysteine-rich protein that affects pathogenesis. *Plant Cell* **6**, 1593-1606.

Dunoyer, P., Pfeffer, S., Fritsch, C., Hemmer, O., Voinnet, O. & Richards, K. E. (2002). Identification, subcellular localization and some properties of a cysteine-rich suppressor of gene silencing encoded by peanut clump virus. *Plant J* **29**, 555-567.

Fernandez-Calvino, L., Guzman-Benito, I., Del Toro, F. J., Donaire, L., Castro-Sanz, A. B., Ruiz-Ferrer, V. & Llave, C. (2015). Activation of senescence-associated dark-inducible genes during infection contributes to enhance susceptibility to plant viruses. *Mol Plant Pathol* doi: 10.1111/mpp.12257.

Fernandez-Calvino, L., Osorio, S., Hernandez, M. L., Hamada, I. B., Del Toro, F. J., Donaire, L., Yu, A., Bustos, R., Fernie, A. R., Martinez-Rivas, J. M. & Llave, C. (2014). Virus-Induced Alterations in Primary Metabolism Modulate Susceptibility to Tobacco rattle virus in Arabidopsis. *Plant Physiol* **166**, 1821-1838.

Garcia-Ruiz, H., Carbonell, A., Hoyer, J. S., Fahlgren, N., Gilbert, K. B., Takeda, A., Giampetruzzi, A., Garcia Ruiz, M. T., McGinn, M. G., Lowery, N., Martinez Baladejo, M. T. & Carrington, J. C. (2015). Roles and Programming of Arabidopsis ARGONAUTE Proteins during Turnip Mosaic Virus Infection. *PLoS Pathog* **11**, e1004755.

Ghazala, W., Waltermann, A., Pilot, R., Winter, S. & Varrelmann, M. (2008). Functional characterization and subcellular localization of the 16K cysteine-rich suppressor of gene silencing protein of tobacco rattle virus. *J Gen Virol* **89**, 1748-1758.

Giner, A., Lakatos, L., Garcia-Chapa, M., Lopez-Moya, J. J. & Burgyan, J. (2010). Viral protein inhibits RISC activity by argonaute binding through conserved WG/GW motifs. *PLoS Pathog* **6**, e1000996.

González, I., Martínez, L., Rakitina, D. V., Lewsey, M. G., Atencio, F. A., Llave, C., Kalinina, N. O., Carr, J. P., Palukaitis, P. & Canto, T. (2010). Cucumber mosaic virus

2b protein subcellular targets and interactions: their significance to RNA silencing suppressor activity. *Mol Plant Microbe Interact* **23**, 294-303.

Hamera, S., Song, X., Su, L., Chen, X. & Fang, R. (2012). Cucumber mosaic virus suppressor 2b binds to AGO4-related small RNAs and impairs AGO4 activities. *Plant J* **69**, 104-115.

Johansen, L. K. & Carrington, J. C. (2001). Silencing on the spot. Induction and suppression of RNA silencing in the Agrobacterium-mediated transient expression system. *Plant Physiol* **126**, 930-938.

Jones-Rhoades, M. W. & Bartel, D. P. (2004). Computational identification of plant microRNAs and their targets, including a stress-induced miRNA. *Mol Cell* **14**, 787-799.

Karlowski, W. M., Zielezinski, A., Carrere, J., Pontier, D., Lagrange, T. & Cooke, R. (2010). Genome-wide computational identification of WG/GW Argonaute-binding proteins in Arabidopsis. *Nucleic Acids Res* **38**, 4231-4245.

Kasschau, K. D., Xie, Z., Allen, E., Llave, C., Chapman, E. J., Krizan, K. A. & Carrington, J. C. (2003). P1/HC-Pro, a viral suppressor of RNA silencing, interferes with Arabidopsis development and miRNA unction. *Dev Cell* **4**, 205-217.

Lakatos, L., Csorba, T., Pantaleo, V., Chapman, E. J., Carrington, J. C., Liu, Y. P., Dolja, V. V., Calvino, L. F., Lopez-Moya, J. J. & Burgyan, J. (2006). Small RNA binding is a common strategy to suppress RNA silencing by several viral suppressors. *EMBO J* **25**, 2768-2780.

Li, J., Reichel, M. & Millar, A. A. (2014). Determinants beyond both complementarity and cleavage govern microR159 efficacy in Arabidopsis. *PLoS Genet* **10**, e1004232.

Lin, S. S., Wu, H. W., Elena, S. F., Chen, K. C., Niu, Q. W., Yeh, S. D., Chen, C. C. & Chua, N. H. (2009). Molecular evolution of a viral non-coding sequence under the selective pressure of amiRNA-mediated silencing. *PLoS Pathog* **5**, e100031.

Liu, D. H., Robinson, D. J., Duncan, G. H. & Harrison, B. D. (1991). Nuclear location of the 16K non-structural protein of tobacco rattle virus. *J Gen Virol* **72 (Pt 8)**, 1811-1817.

Liu, H., Reavy, B., Swanson, M. & MacFarlane, S. A. (2002). Functional replacement of the tobacco rattle virus cysteine-rich protein by pathogenicity proteins from unrelated plant viruses. *Virology* **298**, 232-239.

Llave, C. (2004). MicroRNAs: more than a role in plant development? *Mol Plant Pathol* **5**, 361-366.

Llave, C., Xie, Z., Kasschau, K. D. & Carrington, J. C. (2002). Cleavage of Scarecrow-like mRNA targets directed by a class of Arabidopsis miRNA. *Science* **297**, 2053-2056.

Ma, X., Nicole, M. C., Meteignier, L. V., Hong, N., Wang, G. & Moffett, P. (2015). Different roles for RNA silencing and RNA processing components in virus recovery and virus-induced gene silencing in plants. *J Exp Bot* **66**, 919-932.

Macfarlane, S. A. (2010). Tobraviruses--plant pathogens and tools for biotechnology. *Mol Plant Pathol* **11**, 577-583.

Martin-Hernandez, A. M. & Baulcombe, D. C. (2008). Tobacco rattle virus 16-kilodalton protein encodes a suppressor of RNA silencing that allows transient viral entry in meristems. *J Virol* **82**, 4064-4071.

Martinez-Priego, L., Donaire, L., Barajas, D. & Llave, C. (2008). Silencing suppressor activity of the Tobacco rattle virus-encoded 16-kDa protein and interference with endogenous small RNA-guided regulatory pathways. *Virology* **376**, 346-356.

Niu, Q. W., Lin, S. S., Reyes, J. L., Chen, K. C., Wu, H. W., Yeh, S. D. & Chua, N. H. (2006). Expression of artificial microRNAs in transgenic Arabidopsis thaliana confers virus resistance. *Nat Biotechnol* **24**, 1420-1428.

Palatnik, J. F., Allen, E., Wu, X., Schommer, C., Schwab, R., Carrington, J. C. & Weigel, D. (2003). Control of leaf morphogenesis by microRNAs. *Nature* **425**, 257-263.

Pantaleo, V., Szittya, G. & Burgyan, J. (2007). Molecular Bases of Viral RNA Targeting by Viral Small Interfering RNA-Programmed RISC. *J Virol* **81**, 3797-3806.

Parizotto, E. A., Dunoyer, P., Rahm, N., Himber, C. & Voinnet, O. (2004). In vivo investigation of the transcription, processing, endonucleolytic activity, and functional relevance of the spatial distribution of a plant miRNA. *Genes Dev* **18**, 2237-2242.

Perez-Canamas, M. & Hernandez, C. (2015). Key importance of small RNA binding for the activity of a glycine-tryptophan (GW) motif-containing viral suppressor of RNA silencing. *J Biol Chem* **290**, 3106-3120.

Qi, Y., He, X., Wang, X. J., Kohany, O., Jurka, J. & Hannon, G. J. (2006). Distinct catalytic and non-catalytic roles of ARGONAUTE4 in RNA-directed DNA methylation. *Nature* **443**, 1008-1012.

Qu, F., Ye, X. & Morris, T. J. (2008). Arabidopsis DRB4, AGO1, AGO7, and RDR6 participate in a DCL4-initiated antiviral RNA silencing pathway negatively regulated by DCL1. *Proc Natl Acad Sci U S A* **105**, 14732-14737.

Schott, G., Mari-Ordonez, A., Himber, C., Alioua, A., Voinnet, O. & Dunoyer, P. (2012). Differential effects of viral silencing suppressors on siRNA and miRNA loading support the existence of two distinct cellular pools of ARGONAUTE1. *EMBO J* **31**, 2553-2565.

Schwab, R., Palatnik, J. F., Riester, M., Schommer, C., Schmid, M. & Weigel, D. (2005). Specific effects of microRNAs on the plant transcriptome. *Dev Cell* **8**, 517-527.

Silhavy, D., Molnar, A., Lucioli, A., Szittya, G., Hornyik, C., Tavazza, M. & Burgyan, J. (2002). A viral protein suppresses RNA silencing and binds silencing-generated, 21- to 25-nucleotide double-stranded RNAs. *EMBO J* **21**, 3070-3080.

Simon-Mateo, C. & Garcia, J. A. (2006). MicroRNA-guided processing impairs Plum pox virus replication, but the virus readily evolves to escape this silencing mechanism. *J Virol* **80**, 2429-2436.

560 **Szittya, G., Molnar, A., Silhavy, D., Hornyik, C. & Burgyan, J. (2002).** Short defective
561 interfering RNAs of tombusviruses are not targeted but trigger post-transcriptional gene
562 silencing against their helper virus. *Plant Cell* **14**, 359-372.
563 **Te, J., Melcher, U., Howard, A. & Verchot-Lubicz, J. (2005).** Soilborne wheat mosaic
564 virus (SBWMV) 19K protein belongs to a class of cysteine rich proteins that suppress
565 RNA silencing. *Virol J* **2**, 18.
566 **Todesco, M., Rubio-Somoza, I., Paz-Ares, J. & Weigel, D. (2010).** A collection of target
567 mimics for comprehensive analysis of microRNA function in Arabidopsis thaliana. *PLoS*
568 *Genet* **6**, e1001031.
569 **Vaucheret, H. (2008).** Plant ARGONAUTES. *Trends Plant Sci* **13**, 350-358.
570 **Yelina, N. E., Savenkov, E. I., Solovyev, A. G., Morozov, S. Y. & Valkonen, J. P. (2002).**
571 Long-distance movement, virulence, and RNA silencing suppression controlled by a
572 single protein in hordei- and potyviruses: complementary functions between virus
573 families. *J Virol* **76**, 12981-12991.
574

575 **Figure Legends**

576 **Fig. 1.** 16K does not interfere with the activity of miRNA and viral siRNA pre-assembled
577 RISC complexes. (a) GFP-171.1 was agroinjected with 16K or empty vector (EV). SPMMV
578 P1 and TEV HC-Pro were used as positive and negative controls, respectively. GFP
579 fluorescence was monitored under UV light at 3 dpi. (b) Northern and Western blot analyses
580 in patches infiltrated with GFP-171.1 and constructs expressing silencing suppressors or EV
581 as indicated. (c) GFP fluorescence of Cym 19S-infected recovering leaves infiltrated with
582 GFP-Cym (Cym) or GFP-PoLV (PoLV) sensors and silencing suppressors. (d) Northern and
583 Western blot analyses in Cym19S-infected recovering leaves infiltrated with GFP-Cym or
584 GFP-PoLV sensors and silencing suppressors as indicated. RNA blots were hybridized with
585 DNA radiolabeled probes. Immunoblots were incubated with polyclonal anti-GFP. Ethidium
586 bromide-stained rRNA and Red Ponceau staining were used as RNA and protein loading
587 controls, respectively.

588

589 **FIG. 2.** 16K interferes with assembly of miRNA-guided RISC complexes. (a) Diagrammatic
590 representation of the miR172 complementary region within the 35S-driven GFP-AP2. The
591 miRNA sequence and partial sequence of the validated target mRNA are shown in the
592 expanded area. G-U base pairing is shown (black dots). Nost, NOS terminator (b) GFP
593 fluorescence (3 dpi) in leaves co-infiltrated with GFP-AP2 and each of the miRNA-
594 containing constructs indicated. Patches injected with the cognate miR172 are outlined within
595 an open-box. An empty vector (EV) was used as a negative suppression control. Spots labeled
596 as GFP were infiltrated with a GFP-coding construct alone and were used as controls of
597 fluorescence. Infiltration assays with TEV HC-Pro or 16K are shown. (c) Northern blot assays
598 of GFP-AP2 mRNA in patches co-infiltrated with GFP-AP2 and miR172- or miR171-
599 containing constructs in the presence of 16K, TEV HC-Pro (positive control) or EV (negative

600 control). A GFP DNA radiolabeled probe was used. Ethidium bromide-stained RNA (prior to
601 transfer) is shown as loading control. (d) Gel mobility shift assay for protein-siRNA
602 interactions. Crude protein extracts were incubated with synthetic radiolabeled, double-
603 stranded (ds) 21-nt siRNAs. Leaves injected with P19 and empty vector (EV) were used as
604 positive and negative controls, respectively.
605
606 **Fig. 3.** Host-encoded miRNAs target viral sequences for silencing. (a) Schematic
607 representation of target mRNA complementary regions within the 35S-driven GFP-MCDV
608 and GFP-TRV. The miRNA sequence and partial sequence of the predicted target viral RNA
609 are shown in the expanded area. Mismatches (red dots) and G-U (black dots) base pairing are
610 shown. Nost, NOS terminator (b) Left, GFP fluorescence (3 dpi) in patches co-infiltrated with
611 GFP-MCDV and each of the miRNA-containing constructs indicated. Patches injected with
612 miR172 are outlined within an open-box. An empty vector (EV) was used as a negative
613 control. A GFP expressing construct was used as a control of fluorescence. Infiltration assays
614 with TEV HC-Pro or 16K are shown. Right, Northern blot assays of GFP-MCDV mRNA and
615 miR172 in patches co-infiltrated with GFP-MCDV and EV (-) or miR172 (+). RNA blots
616 were hybridized with radiolabeled probes complementary to GFP or miR172. Ethidium
617 bromide-stained RNA (prior to transfer) is shown as loading control. (c) Left, GFP
618 fluorescence in leaf patches co-infiltrated with a GFP-TRV sensor construct and each of the
619 miRNA-containing constructs indicated. Patches injected with miR399 are outlined.
620 Infiltration assays were conducted as in B. Right, Northern blot assays of GFP-TRV mRNA
621 in patches co-infiltrated with GFP-TRV and EV (-) or miR399 (+).
622
623 **Fig. 4.** Analysis of 16K self-interaction and AGO binding. (a) Visualization of the
624 distribution of fluorescence derived from BiFC in epidermal cells expressing split yellow

625 fluorescence protein (sYFP)-tagged 16K proteins. (b) Left, BiFC-derived fluorescence in
626 tissue co-expressing sYFP-tagged 16K and AGO1 or AGO4 proteins as indicated. The bars
627 represent 75 μm. Right, HA-tagged 16K proteins were immunoprecipitated from leaves co-
628 expressing HA-16K and sYFPN-AGO4. Western blot was done using anti-NtGFP antibody to
629 detect sYFPN-AGO4 and anti-HA antibody to detect HA-16K. (c) Silencing suppressor
630 activity of sYFP-tagged 16K constructs was assessed in leaves co-expressing GFP or GFP
631 plus dsGFP at 5 dpi. A HA-tagged 16K and empty vector (EV) were used as a positive and
632 negative suppression controls, respectively. (d) Left, TRV RNA1 accumulation determined by
633 qRT-PCR in TRV-infected *ago1-27*, *ago2-1* and *ago4-2*. Expression values are relative to
634 that in Col-0 that was arbitrarily set to 1. Asterisks indicate statistical significance versus the
635 control ($P < 0.001$, Duncan's multiple range test). Right, TRV-derived GFP protein
636 accumulation determined by Western blot using an anti-NtGFP antibody. Red Ponceau
637 staining was used as a protein loading control.
638
639 **Fig. 5.** Effect of mutations on conserved Cys-rich motifs within the N-terminus of 16K on
640 protein accumulation and silencing suppression. (a) Alignment of partial amino acid
641 sequences of Cys-rich viral proteins: *Tobravirus* (*Pea early browning virus*, PEBV; *Pepper*
642 *ring spot virus*, PepRSV; TRV) 16K proteins, *Furovirus* (*Chinese wheat mosaic virus*,
643 CWMV) 19K protein, *Hordeovirus* (*Barley stripe mosaic virus*, BSMV) γb protein, and
644 *Pecluvirus* (*Indian peanut clump virus*, IPCV) RNA1 3' terminal gene. Amino acids tested
645 are highlighted in yellow; those common to all sequences are in bold. (b, c) Silencing
646 suppressor activity of sYFPN-tagged 16K constructs in the local transient assay. GFP was co-
647 infiltrated with empty vector (EV) or sYFPN-tagged 16K derivatives as indicated. Northern
648 blot of GFP mRNA was analyzed using a GFP radiolabeled probe at 5 dpi. EV and P19 were
649 used as negative and positive suppression controls, respectively. Ethidium bromide-stained

650 RNA (prior to transfer) is shown as loading control (b). GFP fluorescence was monitored
651 under UV light at 5 dpi (c). (d) Western blot of sYFPN-tagged 16K proteins in agro-
652 inoculated leaves at 3 dpi using an anti-NtGFP antibody. Red Ponceau staining was used as a
653 protein loading control. (e) Western blot of sYFPN-tagged 16K constructs in the presence of
654 empty vector (-) or P19 (+). (f) BiFC assay between sYFPN-tagged 16K derivatives and
655 sYFPC- AGO4 proteins. No BiFC-derived fluorescence was observed. Positive control using
656 sYFPN-16K is shown. The bars represent 75 μm (-16K) or 50 μm (-16K mutants).

Figure 1

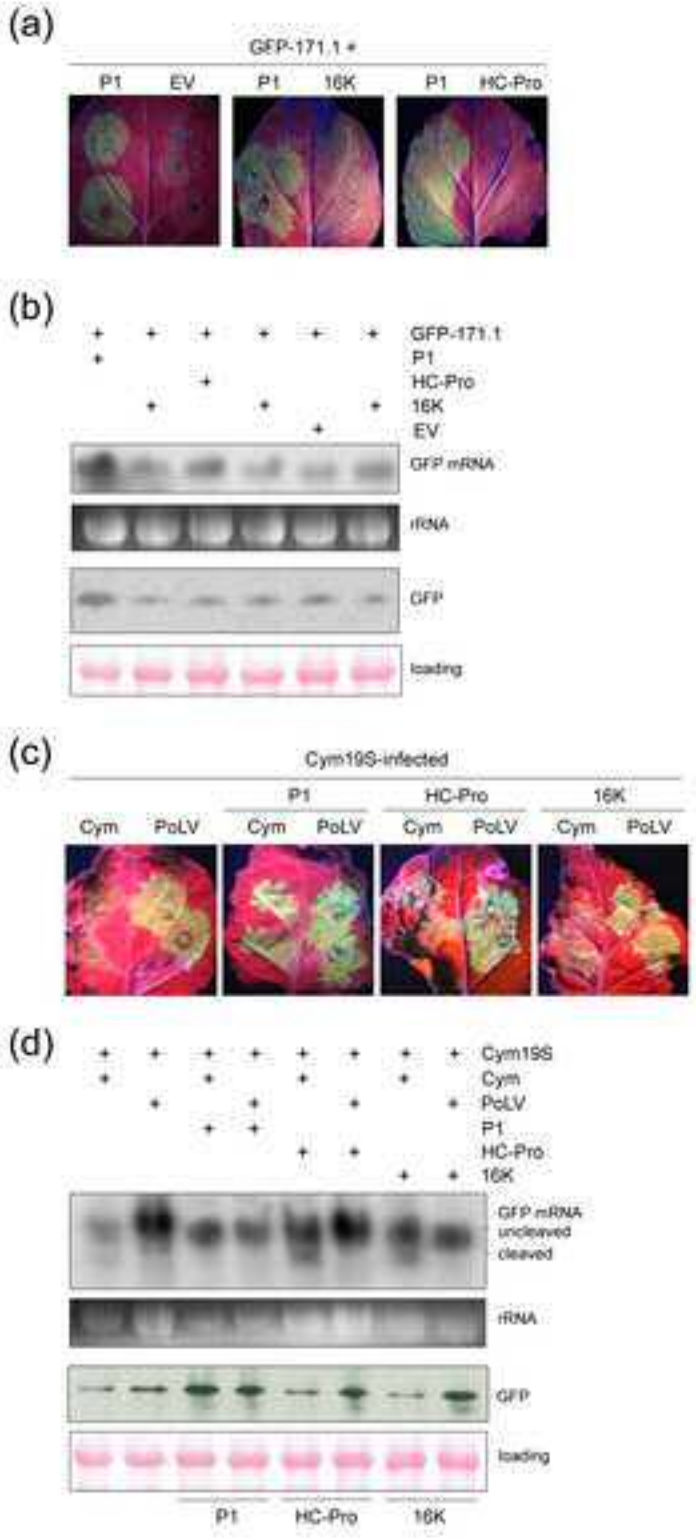

Fernández-Calvino et al. Fig 1

Figure 2

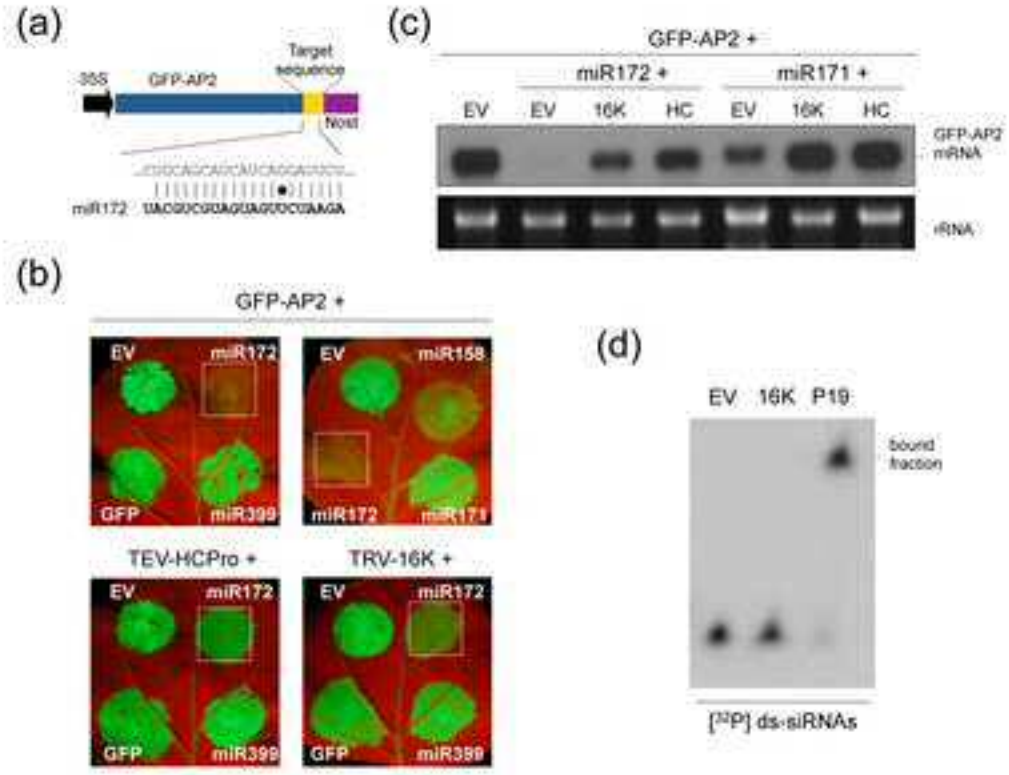

Fernández-Calvino et al. Fig 2

Figure 3

Click here to download Figure Fernandez-Cavino JGV FIG 3.tif

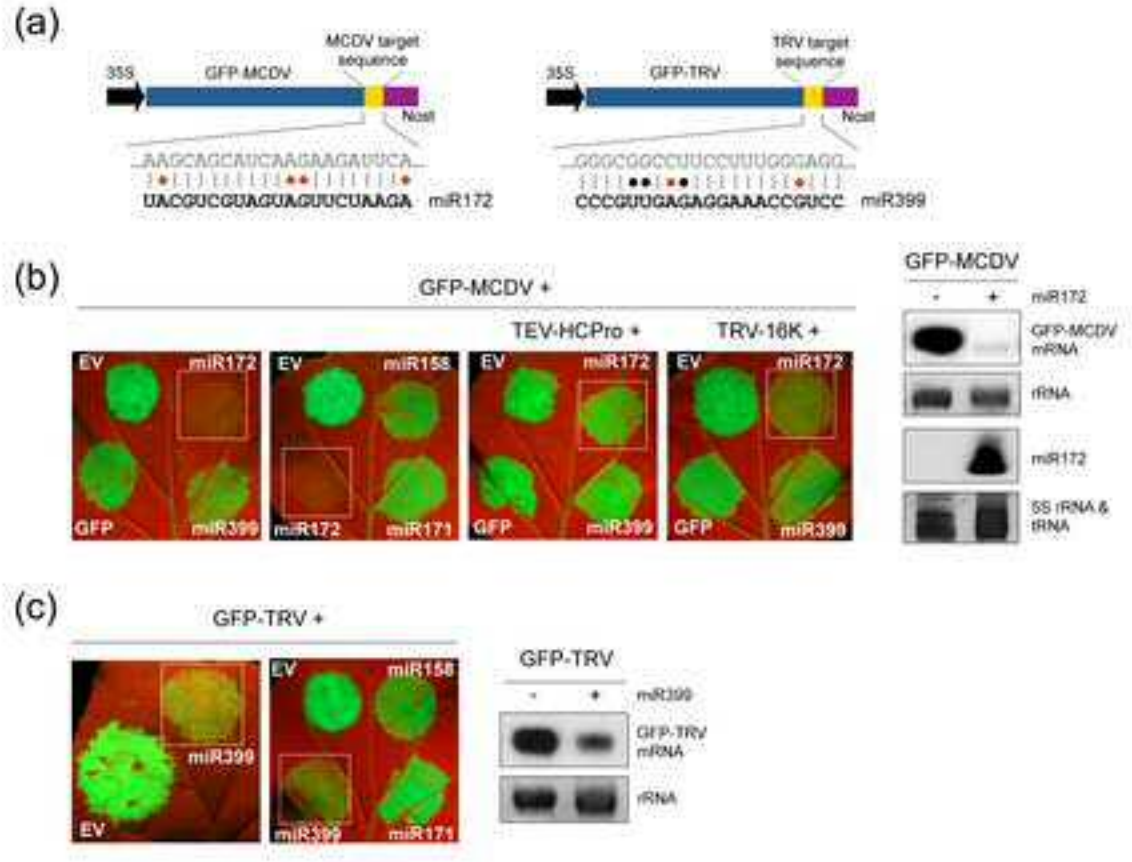

Fernández-Calvino et al. Fig 3

Figure 4

Click here to download Figure Fernandez-Cavino JGV FIG 4.tif

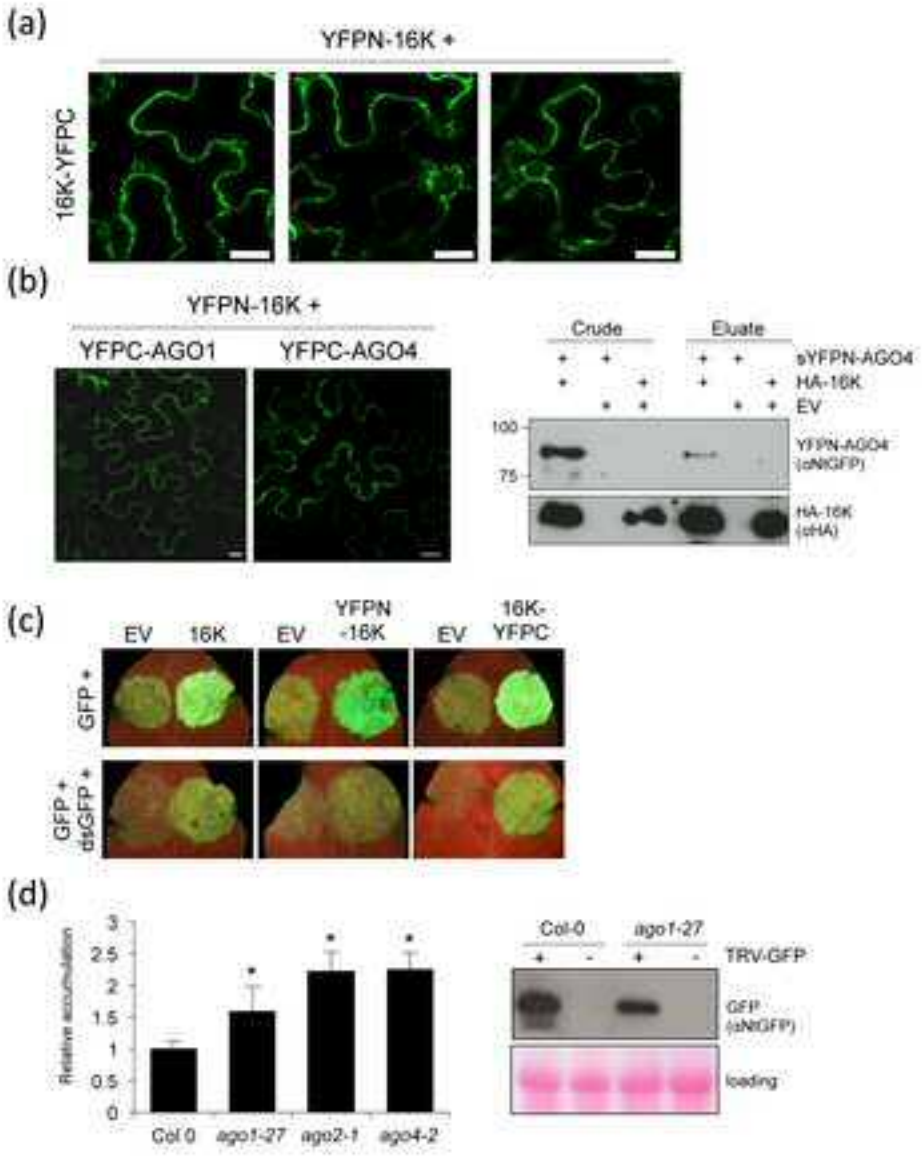

Fernández-Calvino et al. Fig 4

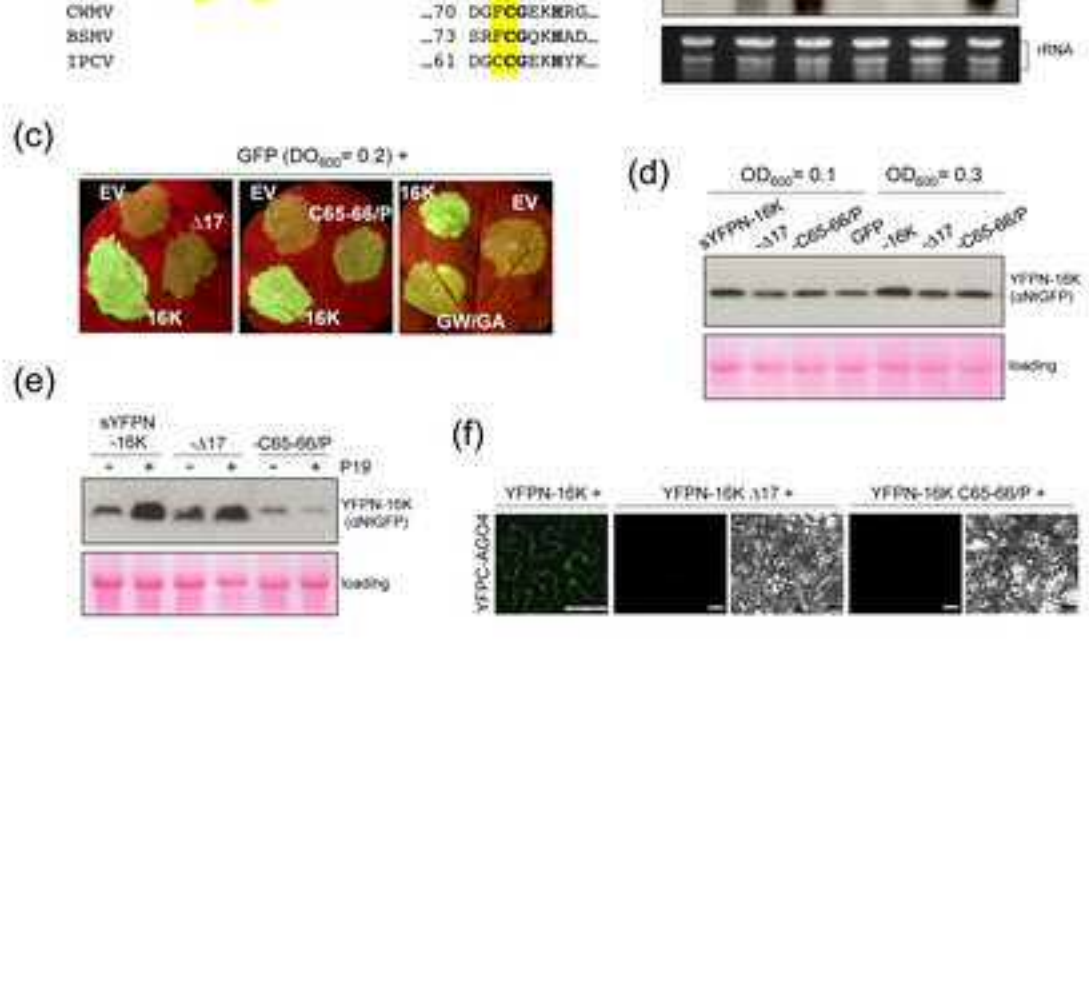

Fernández-Calvino et al. Fig 5

Table S1 List of primers used in this study

Primer	Sequence (5' - 3')	Identifier	Species	Experiment	Restriction site
pre-miR399b-F	CGAGCTCCAAGCCTTCATATGGATCT	MI0001021	Arabidopsis	Cloning	SacI
pre-miR399b-R	GGGGTACCTCAAAGCCGAATAACAGAG	MI0001021	Arabidopsis	Cloning	KpnI
pre-miR172b-F	CGAGCTCCTTCTTCACTTGCACCTCT	MI0000216	Arabidopsis	Cloning	SacI
pre-miR172b-F	GGGGTACCCTTGTAGATGATTGCGTCA	MI0000216	Arabidopsis	Cloning	KpnI
pre-miR158a-F	AGCCATGGCTTTGTCACTTCATACAC	MI0000188	Arabidopsis	Cloning	NcoI
pre-miR158a-F	CGTCTAGACCGGCAATGATGAAGAATG	MI0000188	Arabidopsis	Cloning	XbaI
HA-GFP-F	TATGCCATGGCATACCCTTATGATGTACCTGATTATGCAAGTAAAGGAGAAGAACTTTTC			Cloning	NcoI
GFP-MCDV_R	GCGAGCTCTGAATCTTCTTGATGCTGCTTTTATTTGTATAGTTCATCC			Cloning	SacI
GFP-AP2_R	GCGAGCTCAGAATGCTGATGATGCTGCAGTTATTTGTATAGTTCATCC			Cloning	SacI
GFP-TRV_R	GCGAGCTCCCTCCCAAAGGAAGGCCGCCCTTATTTGTATAGTTCATCC			Cloning	SacI
16K-sYFP-F	CCCGGCATGACGTGTGTACTCAAGGGTTGT		TRV	Cloning	XmaI
16K-sYFP-R	GAGCTCCGTCAAAAAGCAAACAAACGATCAA		TRV	Cloning	SacI
16KC65-66/P-sYFP-F	TGTGTATAATTTTTTTGGCCGTAGTCACCTTG		TRV	Cloning	
16KC65-66/P-sYFP-R	CGGCCAAAAAAATTATACACATCAAAAGTAAAATC		TRV	Cloning	
16KΔ17-sYFP-F	CCCGGGCATGAGTATCGGTCATGCTAAC		TRV	Cloning	
AGO1-sYFP-F	CCCGGGTATGGTGAGAAAGAGAAGAACGGAT	At1g48410	Arabidopsis	Cloning	SmaI
AGO1-sYFP-R	GGTACCTCAGCAGTAGAACATGACACGCT	At1g48410	Arabidopsis	Cloning	KpnI
AGO4-sYFP-F	GGATCCATGGATTCAACAAATGGTAACGG	At2g27040	Arabidopsis	Cloning	BamHI
AGO4-sYFP-R	GGTACCTTAACAGAAGAACATGGAGTTGGC	At2g27040	Arabidopsis	Cloning	KpnI
TUB5-F	GCAACAATGAGCGGTGTGACTT	At1g20010	Arabidopsis	qRT-PCR	
TUB5-R	GAAATGGAGACGAGGGAATGG	At1g20010	Arabidopsis	qRT-PCR	
TRV1-F	GTGCACGCAACAGTTCTAATCG	NC_003805	TRV	qRT-PCR	
TRV1-R	GCTGTGCTTTGATTTCTCCACC	NC_003805	TRV	qRT-PCR	